

Cell Line Classification Using Electric Cell-substrate Impedance Sensing (ECIS)

Megan L. Gelsinger ^{*} Laura L. Tupper [†] David S. Matteson [‡]

May 5, 2022

Abstract

We consider cell line classification using multivariate time series data obtained from Electric Cell-substrate Impedance Sensing (ECIS) technology. The ECIS device, which monitors the attachment and spreading of mammalian cells in real time through the collection of electrical impedance data, has historically been used to study one cell line at a time. We greatly broaden the scope of ECIS by considering simultaneous tracking of multiple cell lines in a search for new methods that can help mitigate the current reproducibility crisis in the biological literature. Our approach capitalizes on the multi-frequency data ECIS provides, which have been underutilized in previous studies. We consider classification of fifteen different mammalian cell lines, construct a dictionary of 29 different characteristic features, and obtain 95% accuracy out-of-sample. Our preliminary findings provide a baseline for future large-scale studies in this field.

Keywords: biophysics, classification analysis, multivariate time series, supervised learning

1 Introduction

Since its introduction in the 1990's [1], ECIS technology has grown in prevalence in the scientific community. The ECIS device utilizes a typical cell culture plate, in which each well is fitted with a gold electrode, allowing for the passage of electrical currents at various AC frequencies. The device then measures the electrical impedance associated with each current, which is unique to each particular cell line (Fig. 1). Impedance, divided into its components resistance and capacitance, is recorded as a function of time, allowing for live monitoring of mammalian cell attachment and spreading.

^{*}Department of Statistical Science, Cornell University

[†]Department of Mathematics and Statistics, Williams College

[‡]Departments of Social Statistics and Statistical Science, Cornell University

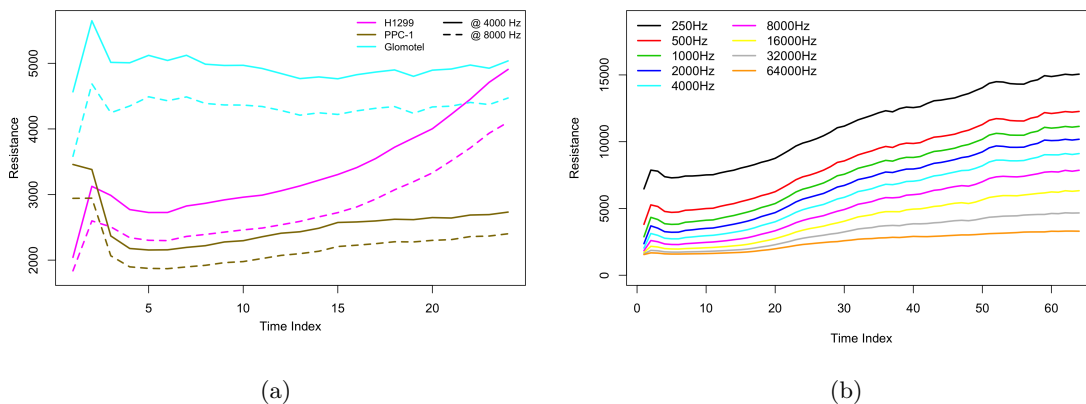


Figure 1: Resistance measurements as recorded by an ECIS device. (a) A unique response for three different cell lines, each exposed to two different AC frequencies. (b) Response of H1299 cell line to all nine AC frequencies.

Various members of the scientific community have incorporated this technology into their studies. Early research focused on showing that ECIS measurements could be associated with known biological characteristics of a particular cell line from the attachment and spreading phases of growth [2, 3]. More recently, others have studied differences in a cell line before and after an event, such as exposure to cytotoxins, finding ECIS an appropriate tool for evaluating induced differences [4, 5]. For a more complete overview of the use of ECIS in the biological literature see [6].

Generally, previous studies have focused on only one cell line at a time, and have neglected exploiting the full potential of the multiple frequency ECIS data. Lovelady et al. (2007) did consider two different cell lines, one cancerous and one healthy, but their analysis relied on only one frequency of data and did not extend to additional cell types [7]. Opp et al. (2009) did consider multiple frequencies in their analysis of cytotoxic effects on cell morphology, but this group limited their use of the multivariate data to a single time index, and for only one cell line [4]. While these approaches have been sufficient for the scope of studies to date, a broader consideration of ECIS data may open greater opportunities, including new approaches for ECIS-based cell line identification.

The main application of ECIS data we consider is cell line classification. Biological studies often rely upon cultured mammalian cells, which are known to mutate and/or become misclassified during the life of an experiment. When such anomalies go unnoticed, erroneous results are reported, contributing to the multi-billion dollar irreproducibility problem [8]. While previous studies, such as those above, have suggested specific features to help characterize single cell lines, none have employed statistical techniques to quantify the ability of potential characteristic features to simultaneously classify multiple cell lines; the typical statistical

analysis in these studies only considered t -tests and F -tests to assess differences in the mean value of a specific feature across populations. This is fundamentally different than performing classification based on a feature, as the latter technique simultaneously assess the characteristic across all populations, and it provides an actual number for how well it separates and identifies the groups. While ultimately we aim to develop an integrated system to perform cell line classification, we limit the scope of this manuscript to a preliminary analysis: extracting many previously considered cell specific ECIS characteristics, assessing them across a much broader domain, and quantifying their classification ability through established statistical techniques.

The remainder of this paper provides the details of our study. In sections two and three, we describe our dataset, feature specification and classification analysis results. In section four, we offer conclusions, and discuss avenues for future work.

2 Data Description

The dataset considered throughout this paper was provided by Applied BioPhysics, the proprietor of ECIS. It consists of fourteen independent replicates of fifteen different mammalian cell lines. Each was exposed to nine different electrical current frequencies over the course of 20 hours, resulting in 64 approximately evenly spaced measurement times. The fifteen different cell lines are: HUTU80, CHOK1, MDCKII, LCELL, WI-38, VA-13, NRK, PPC-1, DuPro, Glomotel, BSC1, DU145, H1299, NIH3T3, and PC-3. The nine AC frequencies measured are: 250, 500, 1000, 2000, 4000, 8000, 16000, 32000, and 64000 Hz. The cells were inoculated in gel serum on a 96 well ECIS device. Each 96 well plate held three different cell lines; for each line, we considered data from one plate. Impedance measurements were recorded approximately once every 20 minutes across all nine AC frequencies. The impedance measurements were decomposed into resistance and capacitance according to the model described in Giaever and Keese [1].

3 Data Analysis

3.1 Technical Review

Many of the characteristics studied in the literature that were suggested to vary by cell line or cell condition were extracted from data obtained during confluence, or the steady-state portion of growth following the initial growth and spreading stages. During this phase, the well is completely covered with cells, allowing for only minute movements. Data collection commonly began after 20-24 hours, once cells had reached confluence, and continued for about 20 hours at a fine sampling frequency, from every two minutes, down to every second. With this resolution of data, researchers were able to extract features such as:

- the slope parameter β characterizing a least-squares straight-line fit to a log-log plot of power spectrum versus frequency ν [3, 4, 5, 7, 9], e.g., Brownian noise displays an ν^{-2} power law, with $\beta = 2$;
- the sample kurtosis, a measure of distributional shape;
- the first $1/e$ crossing of the autocorrelation function of time series from confluence onward, to estimate the exponential decay time [5, 7].

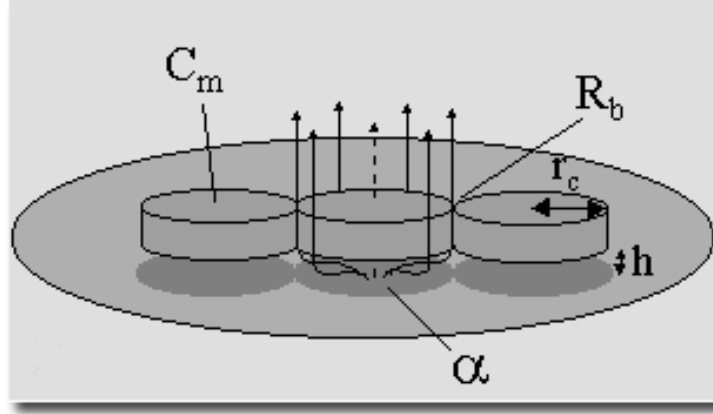


Figure 2: Image obtained from Applied BioPhysics' website (biophysics.com). In the ECIS model, cells are viewed as disks, characterized by parameters R_b , α , r_c , C_m , and h .

Two other confluence level features suggested in previous works were R_b and α (Fig. 2). R_b reflects the barrier resistance between cells, whereas α reflects the constraint on current flow beneath the cells. We define R_b and α by the following relationships:

$$\frac{1}{Z_c(\nu)} = \frac{1}{Z_n(\nu)} \left(\frac{Z_n(\nu)}{Z_n(\nu) + Z_m(\nu)} + \frac{\frac{Z_n(\nu)}{Z_n(\nu) + Z_m(\nu)}}{\frac{i\gamma r_c}{2} \frac{I_0(\gamma r_c)}{I_1(\gamma r_c)} + 2R_b \left(\frac{1}{Z_n(\nu)} + \frac{1}{Z_m(\nu)} \right)} \right);$$

$$\gamma r_c = r_c \sqrt{\frac{\rho}{h} \left(\frac{1}{Z_n(\nu)} + \frac{1}{Z_m(\nu)} \right)} = \alpha \sqrt{\frac{1}{Z_n(\nu)} + \frac{1}{Z_m(\nu)}}.$$

For frequency ν , $Z_c(\nu)$ is the specific impedance (per unit area) of the cell-covered electrode, $Z_n(\nu)$ is the specific impedance of the cell-free electrode, $Z_m(\nu)$ is the specific membrane impedance of the cells, r_c is the radius of the cell, ρ is the resistivity of the solution, h is the height of the space between the ventral surface of the cell and the substrate, and I_0 and I_1 are the modified Bessel functions of the first kind in order 0 and 1 [1]. By recording data over a set of frequencies $\{\nu_1, \dots, \nu_k\}$, we can compute R_b and α . Both [1] and [4] considered R_b and α in their analysis.

Several studies also evaluated features that were specific to the attachment and spreading phases of

growth. In particular, some researchers found that certain cell lines “peaked higher” and “increased more rapidly” during these initial stages of growth [10, 11]. Observations other than these were hard to come by as studies concentrated less on attachment and spreading and more on confluence behavior.

The statistical analysis involved in these studies focused on t -tests and F -tests to assess significant differences in the feature mean across populations of interest. For example, when Opp et al. (2009) considered whether a particular cell population inoculated with varying degrees of a cytotoxin had differing mean R_b values for each dosage level, the authors performed Student’s t -test for two samples with unequal variance, for pairs of dosages, such as 5 μ M versus 10 μ M of cytotoxin [4]. Another example came from the comparison of cancerous and noncancerous cells, in which an F -test was conducted to assess the probability of the two cell lines coming from the same distribution, given the means and variances of their power slopes β [7].

3.2 Feature Specification

The design for our study did not emphasize the confluence stage of growth; only twelve observations (per frequency) were recorded, by sampling wells once every 20 minutes over four hours in the confluence phase. This compares to the thousands of observations available to our counterparts in their studies. Given the lack of data available during this final steady-state stage, we did not extract many of the confluence region features mentioned in Section 3.1. The only exceptions were R_b and α , as they only needed one time index worth of data during the confluence region to compute; at this single time index, the data from all measured frequencies were combined to estimate R_b and α .

To supplement our feature space, we also included proxies for those features from the attachment and spreading portions of cell growth mentioned in Section 3.1. These included:

1. End of run resistance value (EOR);
2. Maximum resistance value (MR);
3. Resistance at two hours (R2h).

Beyond the features described above, we further extended our feature space in a novel way. Previous studies involving these features failed to evaluate them at more than one frequency, typically 4000 Hz. One of the main advantages of ECIS, though, is its ability to record multi-frequency data. Therefore, we evaluated relevant features (EOR, MR, R2h) at all nine measurement frequencies given in Section 2. This gave us a total $(3 \times 9) + 2 = 29$ characteristics in our feature space which we use below to demonstrate the added value of our approach.

3.3 Classification Analysis

Classification algorithms provide predictive accuracy rates which reflect quantitatively how well certain characteristics differentiate the data. In previous ECIS related works, none of these algorithms were used to assess features for cell line classification; instead, F -tests and t -tests were relied upon to merely determine whether the mean value of the feature in question differed by group. We consider a series of classifiers in our study to provide this missing quantitative evaluation of potential characteristics for cell line classification.

Classification analysis was performed using several different supervised learning methods on several different combinations of features. The first “grouping” of features considered was similar to that of previous works, where each feature was analyzed on an individual basis as a tool for cell line differentiation. We also considered all pairs and trios of our 29 features to assess which provide better separation of the data, and if so, by how much. All combinations of features were evaluated with the following classification methods: classification trees, linear discriminant analysis (LDA) and quadratic discriminant analysis (QDA). We will discuss each method and the corresponding results in the remainder of this section.

3.3.1 Classification Trees

We began our analysis with classification trees, as they use the most elementary division of the feature space to classify observations into groups. Classification trees perform an iterated series of binary splits on the data to assign each observation in a given region to the most commonly occurring class of training observations in that region. To create these splits, we select the predictor, or feature, X_j with cutpoint s such that splitting the feature space into regions $\{X|X_j < s\}$ and $\{X|X_j \geq s\}$ leads to the greatest possible reduction in a particular metric. Several different metrics exist for assessing the quality of a particular split, arguably the most common of which is the Gini index, defined by

$$G = \sum_{k=1}^K \hat{p}_{mk}(1 - \hat{p}_{mk}).$$

Here we assume the data can be divided into K classes, with \hat{p}_{mk} representing the portion of training observations in the m th region that are from the k th class. The Gini index, therefore, represents a measure of the total variance across the K classes, which is often referred to as node purity; G assumes small values, or is “pure,” when \hat{p}_{mk} is near zero or one, meaning nearly none or nearly all of the training observations in the m th region are from the k th class, respectively. So, to construct a binary split, we consider all predictors X_1, \dots, X_p at all possible values s , and select the feature and cutpoint such that G is minimized. A classification tree is built by iteratively performing these splits on training data until reaching a specified

node purity threshold. A test set can then be read into the tree, and a predictive accuracy rate computed [12]. We note that based on their definition, the splits in classification trees divide the feature space into a series of half-planes, or rectangles in 2D.

We constructed classification trees on the data, using each single, pair, and trio of features as predictors in separate models. In particular, we randomly split the entire dataset for each cell line in half, using seven of the observations in the training set and the remaining seven in the test set. For each of the 29 individual features, for example, we then constructed classification trees using the `tree()` function in R on the training set and assessed the out-of-sample classification predictive accuracy rate using `predict.tree()` on the test set. We repeated this analysis on twenty different random splits of the data into training and testing sets. Reported accuracy rates for each feature are the average over all twenty of these trials. This procedure was continued with all distinct pairs and trios of features.

Feature Space Dimension	Selected Classification Feature(s)	Out-of-Sample Classification Rate	Approximate Standard Error
1	EOR @ 2000 Hz	0.714	0.009
2	R2h @ 16000 Hz MR @ 8000 Hz	0.932	0.004
3	MR @ 500 Hz R2h @ 16000 Hz MR @ 16000 Hz	0.979	0.003

Table 1: Best feature(s) for cell line classification based on twenty trials of classification tree construction. We recall EOR: End of run resistance; MR: Maximum resistance; R2h: Resistance at two hours. The out-of-sample classification rate in column three is the average over all twenty values obtained for each feature. The standard error of this average value is reported in column four. These results show that when classifying cell lines, a 2D feature space is significantly more informative than a 1D feature space. Using three features as opposed to two results in a less drastic improvement in the out-of-sample classification rate, but an improvement nonetheless.

Table 1 reflects the best feature(s) for classification based on twenty random splittings of the data. Here, EOR, MR, and R2h repeatedly appeared at similar mid to high range frequencies when replicating our procedure. Figure 3 offers a visual of the best pair of features proposed in Table 1, and their ability to separate the data with respect to classification trees.

3.3.2 Linear Discriminant Analysis

Next, we performed classification analysis through the LDA algorithm on all combinations of features, creating a series of linear divisions of the feature space, not necessarily horizontal or vertical, to separate the data. Formally, LDA assumes that observations X of the κ th class are drawn from the multivariate Gaussian distribution with mean vector μ_κ and covariance matrix Σ ($X \sim \text{Normal}(\mu_\kappa, \Sigma)$). Note the lack of subscript on the covariance matrix; LDA assumes that all K classes have the same covariance structure Σ , a

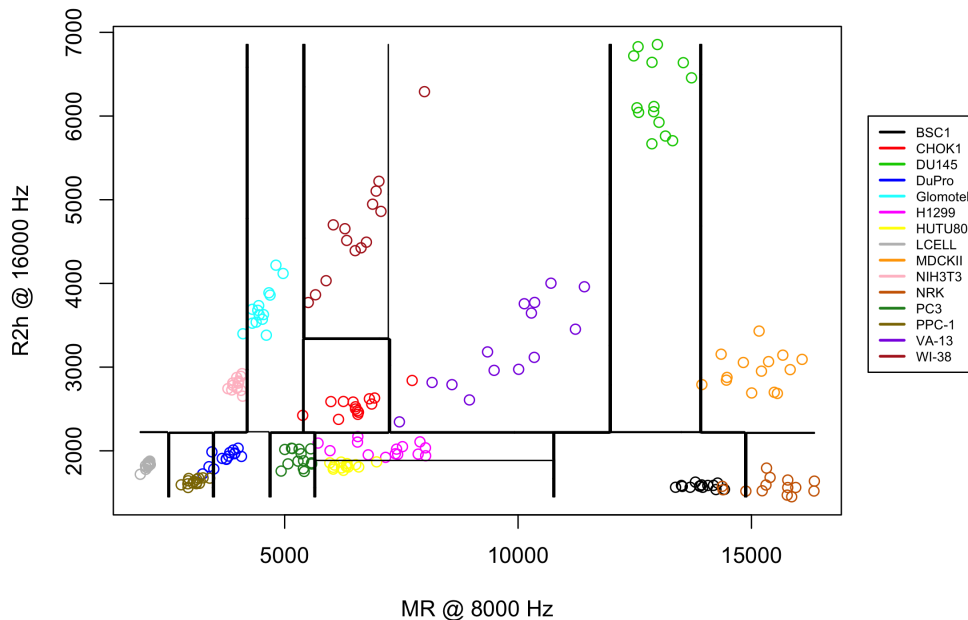


Figure 3: Best pair of features for cell line classification as determined through classification trees. We see most observations of the same color reside in the same rectangular region, indicating good separation. This behavior corresponds to the high classification accuracy ($\approx 93\%$) presented in Table 1.

characteristic which distinguishes this method from other classifiers (see QDA below). The LDA algorithm itself is based on Bayesian analysis. Assuming a Gaussian density for the k th class, the Bayes classifier assigns an observation $X = x$ to the class κ for which the posterior probability of x belonging to the κ th class is maximized. This corresponds to assigning an observation $X = x$ to the class κ for which

$$\kappa = \arg \max_k \delta_k(x) = \arg \max_k [x^T \Sigma^{-1} \mu_k - \frac{1}{2} \mu_k^T \Sigma^{-1} \mu_k].$$

The LDA algorithm estimates μ_k and Σ from the training set, which yields estimates for $\hat{\delta}_k(x)$. An observation $X = x^*$ from the testing set is then assigned to the κ th class if $\kappa = \arg \max_k \hat{\delta}_k(x^*)$. The predicted classes using this scheme can then be compared to the true classes to assess classification accuracy [12].

Just as before, we performed LDA on the data using each single, pair, and trio of features as predictors in separate models. The same random sampling scheme was used, with half of the data constituting the training set, and the other half forming the test set. The `lda()` and `predict.lda()` functions were used to run the analysis and assess the out-of-sample classification predictive accuracy rates. Here too we repeated our analysis on twenty different random samplings of the data to mitigate any sensitivity to initialization.

Reported accuracy rates for each feature are the average over all twenty of these trials.

Feature Space Dimension	Selected Classification Feature(s)	Out-of-Sample Classification Rate	Approximate Standard Error
1	EOR @ 1000 Hz	0.763	0.007
2	R2h @ 2000 Hz MR @ 8000 Hz	0.944	0.004
3	MR @ 64000 Hz R2h @ 1000 Hz MR @ 1000 Hz	0.980	0.003

Table 2: Best feature(s) for cell line classification based on twenty trials of LDA. The out-of-sample classification rate in column three is the average over all twenty values obtained for each feature. The standard error of this average value is reported in column four. Similar features were selected here as in Table 1. The predictive accuracy rates increased for each combination of features, as compared to Table 1. The margin of improvement in this rate decreased slightly between pairs and trios of features.

Figure 4 depicts the linear division of the feature space characteristic of LDA. Note that while these divisions are quite different from those in Figure 3, the classification accuracy rates in Table 2 are only slightly higher than those in Table 1. We also see that similar trends in the selected best features carry over from classification trees to LDA. EOR, R2h, and MR are the dominant features, as are the mid-range measurement frequencies. The predictive accuracy rates increase across all combinations of features, but the margin of improvement between pairs and trios of features decreases slightly.

3.3.3 Quadratic Discriminant Analysis

Finally, we performed QDA to allow for quadratic divisions of the feature space for classification. QDA is similar to LDA; QDA assumes that observations X of the κ th class are drawn from the multivariate Gaussian distribution with mean vector μ_k and covariance matrix Σ_k ($X \sim \text{Normal}(\mu_k, \Sigma_k)$). Here too the Bayes classifier assigns an observation $X = x$ to the class κ for which the posterior probability of x belonging to the κ th class is maximized. This corresponds to assigning an observation $X = x$ to the class κ for which

$$\kappa = \arg \max_k \delta_k(x) = \arg \max_k \left[-\frac{1}{2}(x - \mu_k)^T \Sigma_k^{-1} (x - \mu_k) \right].$$

Notice here that each of the $k = 1, \dots, K$ classes has its own distinct covariance function, and that the observation x appears in a quadratic form in the Bayes classifier. These are the defining characteristics of QDA. The QDA algorithm estimates μ_k and Σ_k from the training set, which yields estimates for $\hat{\delta}_k(x)$. An observation $X = x^*$ from the testing set is then assigned to the κ th class if $\kappa = \arg \max_k \hat{\delta}_k(x^*)$. The predicted classes using this scheme can then be compared to the true classes to assess classification accuracy [12].

The same procedures for testing classification trees and LDA on the data were used for QDA. The

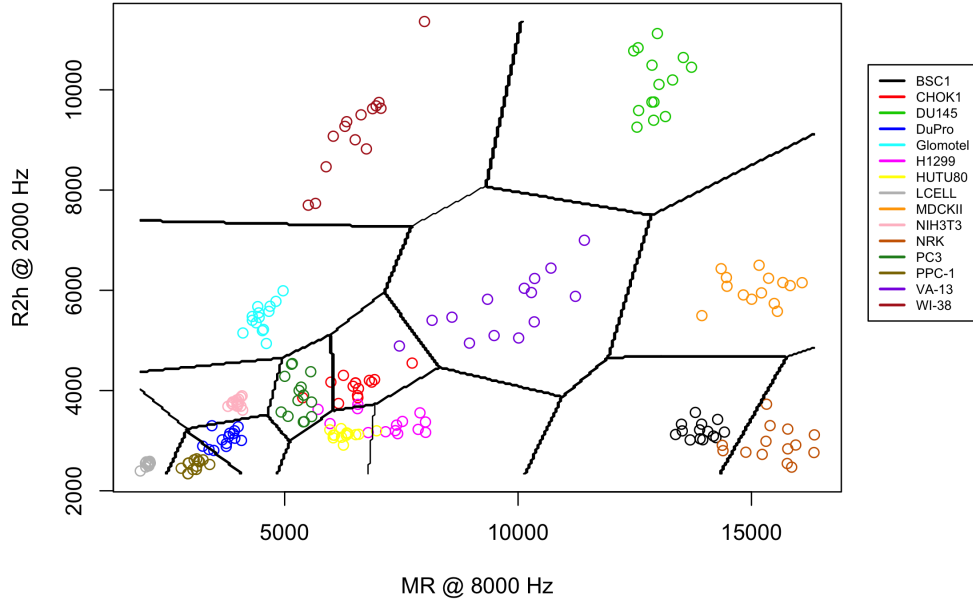


Figure 4: Best pair of features for cell line classification as determined through LDA. We see most observations of the same color reside in the same oblong region, indicating good separation. This behavior corresponds to the high classification accuracy ($\approx 94\%$) presented in Table 2.

functions utilized in R were `qda()` and `predict.qda()`. Table 3 contains the out-of-sample predictive accuracy rates given the fitted QDA models. Figure 5 depicts the quadratic division of the feature space for the best pair of characteristics in Table 3. While these boundaries look quite different from those in Figure 3 and Figure 4, we see only minor differences in their predictive accuracies, especially between LDA and QDA.

Feature Space Dimension	Selected Classification Feature(s)	Out-of-Sample Classification Rate	Approximate Standard Error
1	EOR @ 1000 Hz	0.745	0.007
2	R2h @ 32000 Hz MR @ 8000 Hz	0.949	0.004
3	EOR @ 16000 Hz R2h @ 8000 Hz R2h @ 4000 Hz	0.983	0.005

Table 3: Best feature(s) for cell line classification based on twenty trials of QDA. The out-of-sample classification rate in column three is the average over all twenty values obtained for each feature. The standard error of this average value is reported in column four. These results are almost identical to those from LDA.

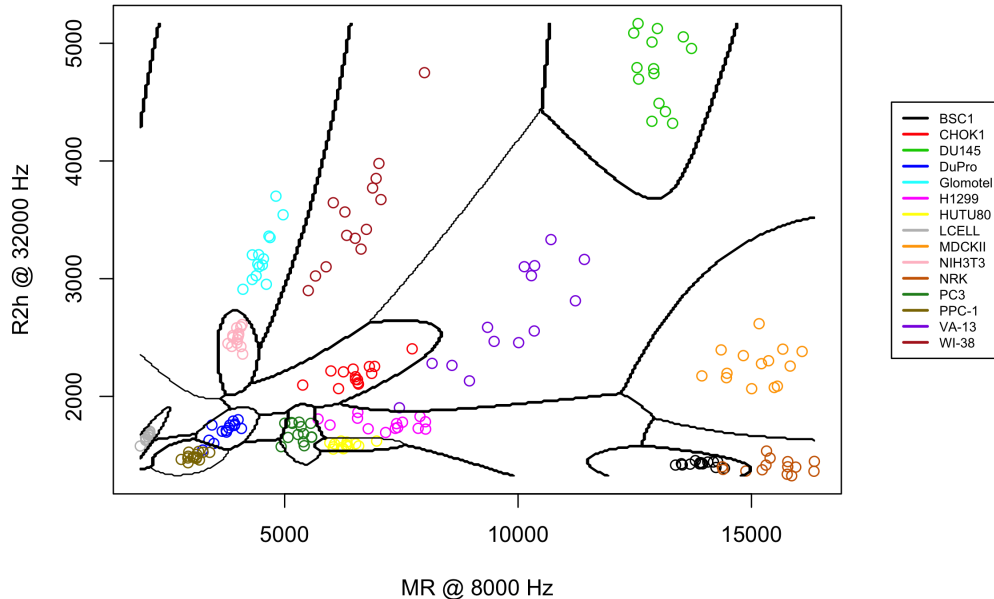


Figure 5: Example of best pair of features for cell line classification as determined through QDA. This separation corresponds to about 95% predictive accuracy, as seen in Table 3.

4 Conclusions

Our analysis revealed several key sights. First, we established that previous studies were missing valuable information by only relying on ECIS data obtained from one frequency, typically 4000 Hz. While the tables in this manuscript provide just some examples of the best feature(s), it was consistent that 4000 Hz was not the sole frequency selected. We also found that previous works were limiting the scope of the features for cell line differentiation by analyzing them on an individual basis. While only incremental improvement in accuracy was gained from considering trios of features, as opposed to pairs of features, there was a marked improvement by considering pairs versus individual features in this experiment. As for the best classification method, our results suggest that while LDA and QDA might be slightly better algorithms for this data, with small improvements over basic classification trees.

Overall, results are encouraging for future work. Since we now know the value of utilizing the multi-frequency data offered by ECIS for cell line classification, we will look to extend the experimental design to allow for a broader feature space. In particular, we will look for cells grown on different serums within the well, and for cells wounded by a high frequency current after reaching confluence [6]. We will also obtain more data at a finer temporal resolution during the steady-state stage of growth to study those confluence

features proposed in previous studies that we were unable to address in this work. As done in this study, we will evaluate each feature, both new and old, at multiple frequencies to maximize our information basis. Together, we hope these features will enrich the classification algorithm and provide even better cell line separation. Lastly, we note the potential for a two or three dimensional final feature space which provides good classification accuracy given our results, making a visualization tool of this classification scheme feasible.

5 Acknowledgements

The authors would like to thank Applied BioPhysics for providing the data and the technical/biological background for this work. Financial support from the Cornell University Institute of Biotechnology, the New York State Division of Science, Technology and Innovation (NYSTAR), a Xerox PARC Faculty Research Award, NSF Award DMS-1455172 and Cornell University Atkinson’s Center for a Sustainable Future AVF-2017 is gratefully acknowledged as well.

References

- [1] Ivar Giaever and Charles R Keese. Micromotion of mammalian cells measured electrically. *Proceedings of the National Academy of Sciences*, 88(17):7896–7900, 1991.
- [2] Paramitra Mitra, Charles R Keese, and Ivar Giaever. Electric measurements can be used to monitor the attachment and spreading of cells in tissue culture. *BioTechniques*, 11(4):504–510, 1991.
- [3] Chun-Min Lo, Charles R Keese, and Ivar Giaever. Monitoring motion of confluent cells in tissue culture. *Experimental cell research*, 204(1):102–109, 1993.
- [4] Daniel Opp, Brian Wafula, Jennifer Lim, Eric Huang, Jun-Chih Lo, and Chun-Min Lo. Use of electric cell–substrate impedance sensing to assess in vitro cytotoxicity. *Biosensors and Bioelectronics*, 24(8):2625–2629, 2009.
- [5] Douglas C Lovelady, Jennifer Friedman, Sonali Patel, David A Rabson, and Chun-Min Lo. Detecting effects of low levels of cytochalasin b in 3t3 fibroblast cultures by analysis of electrical noise obtained from cellular micromotion. *Biosensors and Bioelectronics*, 24(7):2250–2254, 2009.
- [6] Sonja Lukic and Joachim Wegener. Impedimetric monitoring of cell-based assays. *eLS*, 2015.

- [7] Douglas C Lovelady, TC Richmond, Anastasia N Maggi, Chun-Min Lo, and David A Rabson. Distinguishing cancerous from noncancerous cells through analysis of electrical noise. *Physical Review E*, 76(4):041908, 2007.
- [8] Leonard P Freedman, Iain M Cockburn, and Timothy S Simcoe. The economics of reproducibility in preclinical research. *PLoS biology*, 13(6):e1002165, 2015.
- [9] Angelika Sapper, Joachim Wegener, and Andreas Janshoff. Cell motility probed by noise analysis of thickness shear mode resonators. *Analytical chemistry*, 78(14):5184–5191, 2006.
- [10] Irene H Heijink, Simone M Brandenburg, Jacobien A Noordhoek, Dirkje S Postma, Dirk-Jan Slebos, and Antoon JM van Oosterhout. Characterisation of cell adhesion in airway epithelial cell types using electric cell–substrate impedance sensing. *European Respiratory Journal*, 35(4):894–903, 2010.
- [11] Giljun Park, Chang K. Choi, Anthony E. English, and Tim E. Sparer. Electrical impedance measurements predict cellular transformation. *Cell Biology International*, 33(3):429–433, 2009.
- [12] Gareth James, Daniela Witten, Trevor Hastie, and Rob Tibshirani. *An Introduction to Statistical Learning*. Springer, 2013.